Journal of Balkan Science and Technology
journal homepage: www.jbst.nku.edu.tr/

Enhancing Physical Properties: Chromium-Doped Zinc Oxide Thin Films Deposited by Ultrasonic Spray Pyrolysis

Ibrahim GUNES[1*], Emrah SARICA[2], Vildan BILGIN[3]

[1] *Canakkale Onsekiz Mart University, Department of Electricity and Energy, Canakkale, Türkiye*
[2] *Baskent University, Department of Electrical and Electronics Engineering, Ankara, Türkiye*
[3] *Canakkale Onsekiz Mart University, Department of Physics, Canakkale, Türkiye*

Research Article

Keywords:
Chromium-doped ZnO thin films
Ultrasonik spray pyrolysis
Physical properties

Received: 31.07.2023
Accepted: 17.08.2023
Published: 31.08.2023

DOI: 10.55848/jbst.2023.34

ABSTRACT

In this study, undoped and different concentrations (3%, 6%, and 9%) of chromium-doped ZnO thin films were deposited using the ultrasonic spray pyrolysis technique, and the significant effects of the dopant concentration on the physical properties of the deposited films, including structural, morphological, and electrical characteristics, were investigated. The structural analysis revealed that the thin films possessed a hexagonal wurtzite structure, and the intensity of the peak corresponding to the (002) plane initially increased with the increasing dopant concentration, then decreased, and increased again. Morphological analysis showed that there were no regular changes in the crystal sizes with increasing dopant concentration, but noticeable alterations occurred on the film surfaces. The optical band gaps of the deposited films increased from 3.24 eV to 3.31 eV with the increasing dopant concentration. The electrical resistivity values of the films varied between 3.04×10^{1} Ωcm and 3.35×10^{6} Ωcm, indicating that higher dopant concentrations led to an increase in resistivity.

1. Introduction

Zinc oxide (ZnO) is a binary semiconductor oxide belonging to the II-VI group and is highly investigated both in bulk and nanostructured forms due to its versatile properties [1–3]. With a hexagonal wurtzite crystal structure, this compound exhibits n-type electrical conductivity inherently, mainly due to structural defects such as Zn interstitial atoms and O vacancies [4]. Moreover, it possesses a direct bandgap of around 3.3 eV and a high exciton binding energy of 60 meV at room temperature [4–6]. These characteristics make ZnO an excellent candidate for optoelectronic applications. Particularly, the high exciton binding energy helps to lower the threshold energy and achieve high radiative efficiency in UV laser applications. This feature makes ZnO materials suitable for devices that emit radiation in the UV region [7]. Additionally, its abundance in nature leads to cost-effectiveness, and its properties, such as high optical transparency and high electrical resistivity control, as well as its non-toxic nature, give ZnO advantages over other metal oxide semiconductors like In_2O_3 and SnO_2 [8–10]. Consequently, ZnO becomes a favorable choice for various applications.

Doping ZnO with different metal ions can further modify its suitability for various application areas by enhancing electrical conductivity (Al, Ga, Cl, I, etc.), achieving p-type conductivity (Li, Na, P, Sb, etc.), and inducing room temperature ferromagnetic properties with transition metals (Mn, Fe, Co, Ni, etc.). These modifications open up various application areas for ZnO [11–13]. One of the metal ions used for doping is chromium (Cr), which can exist in different valence states (2+, 3+, and 6+) and forms various ions. In particular, Cr^{3+} ions have a similar ionic radius (Zn=0.74 Å, Cr=0.63 Å) to Zn^{2+} ions, making them easily incorporable into the ZnO crystal lattice or readily substituting Zn ions within the crystal [1,2,14]. Therefore, it can be said that chromium doping significantly affects the physical properties of ZnO films.

ZnO films are grown using various physical vapor deposition techniques as well as solution-based methods in the literature [15,16]. Among these techniques, the ultrasonic spray pyrolysis (USP) technique stands out due to its simplicity, relatively low cost, and significant advantages compared to many other film growth methods. One of the most crucial advantages is that the properties of the grown materials can be controlled and modified by appropriately adjusting the spray conditions. These advantages are essential for the development of technological applications. In this study focuses on the growth of undoped and different concentrations (3%, 6%, and 9%) of chromium-doped ZnO films using the ultrasonic spray pyrolysis technique to enhance their physical properties.

2. Material and Method

2.1. Deposition of ZnO:Cr Thin Films

Undoped and different concentrations (3%, 6%, and 9%) of chromium-doped ZnO thin films were deposited onto glass substrates using the ultrasonic spray pyrolysis technique. Initially, a two-step cleaning procedure was applied to the glass

[*] *Çanakkale Onsekiz Mart Üniversitesi, Biga Meslek Yüksekokulu, Elektrik ve Enerji Bölümü, Prof. Dr. Ramazan AYDIN Yerleşkesi, 17200, Biga-Canakkale, Türkiye*
E-mail address: ibrahimgunes@comu.edu.tr

substrates using an ultrasonic bath, with each step lasting 20 minutes. The cleaning steps involved washing with detergent-mixed deionized (DI) water, followed by rinsing with only DI water. Subsequently, 0.1 M spray solutions were prepared from zinc acetate [$Zn(CH_3COO)_2.2H_2O$] and chromium chloride [$CrCl_3.6H_2O$] salts. The prepared spray solutions were atomized using an ultrasonic nozzle at a flow rate of 5 ml/min and a working frequency of 100 kHz. The atomized solutions were sprayed onto the preheated substrates at 350°C using compressed air at 1 bar pressure for 30 minutes. The distance between the ultrasonic nozzle and the heating plate was set to 35 cm. For convenience during the investigation of the physical properties of the thin films, the undoped and 3%, 6%, and 9% chromium-doped ZnO films were labeled as ZC-0, ZC-3, ZC-6, and ZC-9, respectively.

2.2. Characterization of ZnO:Cr Thin Films

The thicknesses of the thin films were determined using the PHE-102 Spectroscopic Ellipsometer (SE) instrument. The thicknesses of the undoped and 3%, 6%, and 9% chromium-doped ZnO thin films were measured as 332 nm, 312 nm, 328 nm, and 399 nm, respectively. The structural analysis of the thin films was performed by obtaining the X-ray diffraction (XRD) patterns using a PANalytical Empyrean X-ray diffractometer. CuKα radiation with a wavelength of 1.5405 Å was used, and the scan range was set between 20° and 80° (2θ) with a step size of 0.013°. The surface morphology and roughness of the thin films were examined using a Park System XE 70 model Atomic Force Microscope (AFM) in non-contact mode at room temperature. Additionally, the surface morphology of the thin films was analyzed from the Scanning Electron Microscope (SEM), SEM images obtained using a JEOL JSM-7100-F. Elemental analyses of the thin films were performed simultaneously using Energy Dispersive X-ray Spectroscopy (EDS) through an EDS detector. The optical analyses of the thin films were conducted by obtaining the transmission, absorption, and reflection spectra in the wavelength range of 200-900 nm using a Shimadzu UV-2600 model spectrophotometer. For the electrical analysis of the thin films, electrical resistivity values were measured at room temperature using the Lucas Labs Pro4 four-probe system.

3. Results and Discussion

3.1. XRD Analysis

The XRD patterns obtained for undoped and different concentrations of Cr-doped ZnO thin films are presented in Fig. 1. These diffraction patterns exhibit a good agreement with the hexagonal wurtzite structure of ZnO (JCPDS Card No: 36-1451). The presence of multiple peaks in the XRD patterns indicates that the thin films possess a polycrystalline structure, while the sharp, narrow, and intense peaks suggest a high degree of crystallinity. For ZC-0 and ZC-3 thin films, six distinct peaks corresponding to (100), (002), (101), (110), (103), and (112) crystallographic planes were observed at approximately 2θ values of 32.2°, 34.8°, 36.7°, 57.0°, 63.3°, and 68.3°, respectively. With an increasing Cr doping concentration in ZC-6 and ZC-9 thin films, an additional peak attributed to the (102) plane appeared at around 2θ = 48.0°. However, for all the deposited thin films except ZC-9, it was found that all the peaks belonged to the ZnO phase, and there was no evidence of a different phase likely to be formed by the dopant atoms. In contrast, for the ZC-9 thin film, a peak related to the chromium oxide compound phase of Cr_2O_3 (JCPDS Card No: 06-0504) was observed at around 2θ=23.0°. Additionally, the peak intensity corresponding to the (002) plane initially increased and then decreased with an increasing doping concentration. The variation in peak intensities associated with other planes showed an inverse relationship with the intensity of the (002) plane. The relationship between the calculated texture coefficients (TC) for each peak, as given in Table 1, and the changes in peak intensities is evident.

$$TC_{(hkl)} = \frac{I_{(hkl)}/I_{0_{(hkl)}}}{1/N[\sum I_{(hkl)}/I_{0_{(hkl)}}]} \quad (1)$$

where $I_{(hkl)}$ is the intensity value of the corresponding diffraction peak, $I_{0(hkl)}$ is the standard intensity value obtained from the JCPDS card, and N is the number of diffraction peaks. As seen in Table 1, the (002) preferred orientation is evident in the ZC-3 thin film, while in the ZC-0 & ZC-6 thin films, growth is dominant along the (100), (002), and (110) orientations, and in the ZC-9 thin film, growth is dominant along the (100), (002), and (102) orientations. The crystal size was determined using the Debye-Scherrer equation [17], based on the positions and full-width half-maximum (FWHM) values of the diffraction peaks, and these values are provided in Table 1.

$$D = \frac{(0.94)\lambda}{\beta cos\theta} \quad (2)$$

where D is the crystallite size, λ is the wavelength of the X-rays used, β is the full-width half- maximum (FWHM) in radians, and θ is the Bragg angle in radians. In all the deposited films, the crystallite sizes varied between 22 nm and 15 nm, considering the dominant orientation. Consequently, there was no consistent change observed in FWHM and, thus, in crystallite sizes with respect to the increasing dopant concentration.

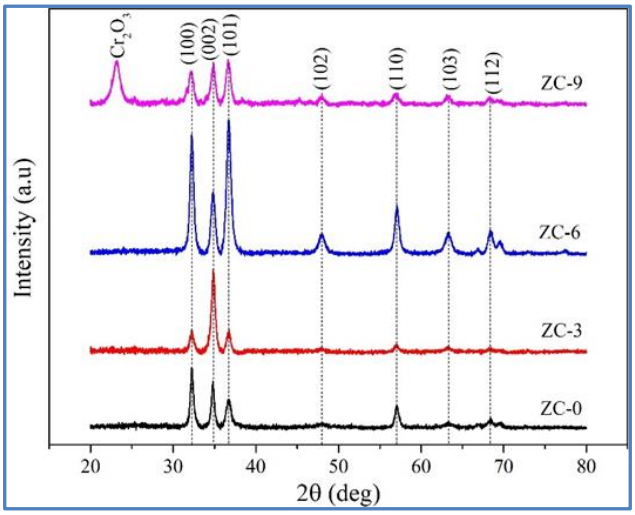

Fig. 1 XRD patterns of ZnO:Cr thin films.

Table 1. Diffraction angles (*2θ*), Miller indices (*hkl*), full-width half-maxima (*β*), texture coefficient (*TC*), crystallite size (*D*), lattice constants (*a* and *c*), c/a ratio and unit cell volume (*V*) of ZnO:Cr thin films.

Sample	2θ(°)	(hkl)	β (°)	TC	D(Å)	a (Å)	c (Å)	c/a	V (Å^3)
ZC-0	32.19	(100)	0.4080	1.41	211	3.219	5.151	1.600	46.25
	34.82	(002)	0.3847	1.53	225				
	36.64	(101)	0.6589	0.54	132				
	57.03	(110)	0.5302	1.04	178				
	63.30	(103)	1.3117	0.58	74				
	68.43	(112)	0.7876	0.89	127				
ZC-3	32.26	(100)	0.5598	0.98	154	3.210	5.149	1.603	45.98
	34.84	(002)	0.5582	2.59	156				
	36.73	(101)	0.6344	0.51	137				
	57.03	(110)	0.6642	0.65	142				
	63.31	(103)	0.9025	0.58	108				
	68.28	(112)	0.7349	0.68	136				
ZC-6	32.19	(100)	0.4814	1.35	179	3.218	5.153	1.601	46.24
	34.81	(002)	0.6115	1.21	142				
	36.65	(101)	0.5998	0.91	145				
	48.05	(102)	0.8925	0.87	101				
	57.16	(110)	0.5925	1.01	159				
	63.30	(103)	0.9325	0.67	104				
	68.34	(112)	0.7638	0.95	131				
ZC-9	32.32	(100)	0.6793	1.04	127	3.228	5.146	1.593	46.45
	34.86	(002)	0.5794	1.64	150				
	36.57	(101)	0.67949	0.71	128				
	48.01	(102)	0.6374	1.21	142				
	56.96	(110)	0.8533	0.75	110				
	63.29	(103)	0.7375	0.76	132				
	68.23	(112)	0.7986	0.84	125				

The lattice constants and unit cell volume for materials with a hexagonal crystal structure were calculated using the equations provided below [17].

$$\frac{1}{d^2} = \frac{4}{3}\left(\frac{h^2+hk+k^2}{a^2}\right) + \left(\frac{l^2}{c^2}\right) \quad (3)$$

$$V = \frac{\sqrt{3}}{2}a^2c \quad (4)$$

where *d* is the interplanar spacing, *V* is the unit cell volume, *h*, *k*, and *l* are Miller indices, and *a* and *c* are lattice constants. As seen in Table 1, when compared with the values obtained from JCPDS Card No: 36-1451 (a=b=3.249 Å, c=5.206 Å, and V=47.62), the values for the deposited films are relatively low. Additionally, the ratio of lattice constants (c/a) for an ideal ZnO hexagonal crystal structure is approximately 1.63. The films deposited showed a c/a ratio around 1.60, and these two values

are found to be in good agreement with each other. Despite studies suggesting that high Cr content (as Cr_2O_3) generally impedes the growth of ZnO crystallites, practical observations reveal the opposite [18]. This discrepancy can be attributed to the ability of Cr doping to reduce the c lattice parameter of the ZnO structure. This reduction in the lattice constant affects the lattice strain and, contrary to expectations, leads to an increase in the crystallite size [18–21].

3.2. Morphological and Compositional Analysis

Atomic force microscopy (AFM) and scanning electron microscopy (SEM) were used to analyze the surface properties of the deposited thin films. The 3-D AFM images of the thin films are shown in Fig. 2(a-d). Upon examining the AFM images, the presence of dark and bright regions is noticeable in all the films. The dark regions represent the formation of pits on the film surfaces, while the bright regions represent the formation of peaks that could result from the stacking of particles, possibly due to island-type growth mechanisms. It is evident that the grains observed on the surface of the ZC-3 thin film are of smaller size compared to the ZC-0 thin films. Furthermore, the sizes of the grains on the surface of the ZC-9 thin films appear to be similar to those of the ZC-6 thin films. This indicates that there is no systematic change in the grain sizes with an increasing doping concentration. Additionally, using the AFM images, the average surface roughness values (Ra) of the deposited thin films were determined to be 13 nm, 9 nm, 16 nm, and 32 nm for undoped, ZC-3, ZC-6, and ZC-9 thin films, respectively. In this regard, it can be stated that the increased roughness of the ZC-9 thin film and its distinct surface appearance compared to the surfaces of other films can be attributed to a noticeable change in the surface properties of the thin films with an increasing Cr doping.

SEM images at x30K magnification of undoped and different concentrations of Cr-doped ZnO thin films are presented in Fig. 3(a-d). These images reveal that the surfaces of ZC-0 and ZC-3 thin films consist of homogeneously distributed grains with varying sizes, tightly packed in an orderly arrangement. This suggests that these thin films exhibit a well-formed structure and good adhesion to the substrate. On the other hand, upon examining the images of ZC-6 and ZC-9 thin films, it is observed that their surfaces exhibit formations of different forms compared to ZC-0 and ZC-3 thin films. In this regard, it can be inferred that a high concentration of Cr doping leads to noticeable changes in both the surface morphology and structural properties of ZnO thin films

Energy Dispersive X-ray Spectroscopy (EDS) was used for the elemental analysis of the deposited thin films. The EDS spectra of the thin films are shown in Fig. 4(a-d). Upon examination of these spectra, it is observed that the expected peaks corresponding to Zn and O atoms are present. . On the other hand, it has been determined that the other peaks seen in the spectra originate from elements such as Mg, Ca, and Si, which are present in the microscope slides used as substrates. From the intensities of the peaks in the spectra, it is evident that there is a higher proportion of Zn atoms compared to O atoms in the structure.

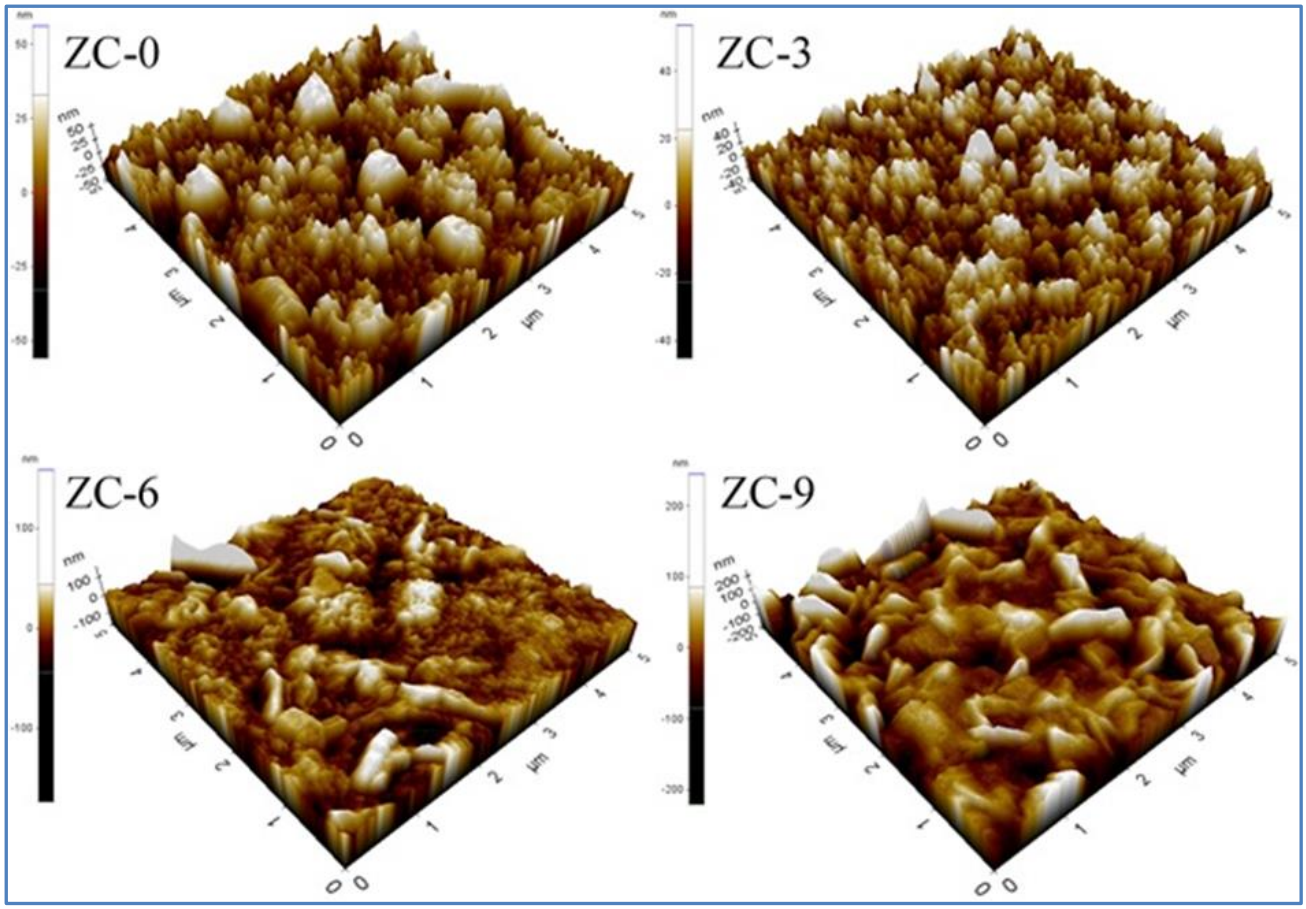

Fig. 2 AFM image of ZnO:Cr thin films.

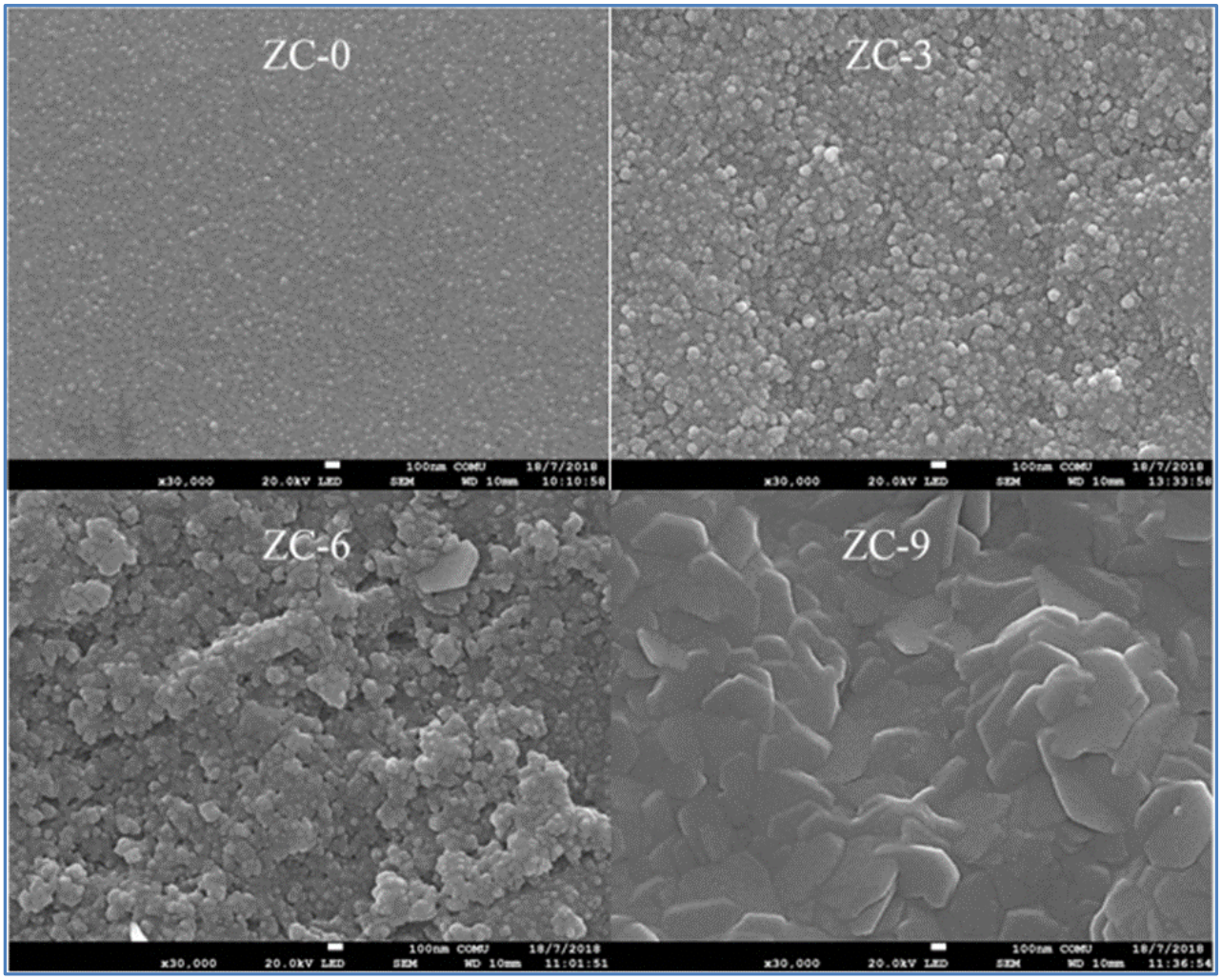

Fig. 3 30K magnified SEM images of ZnO:Cr thin films.

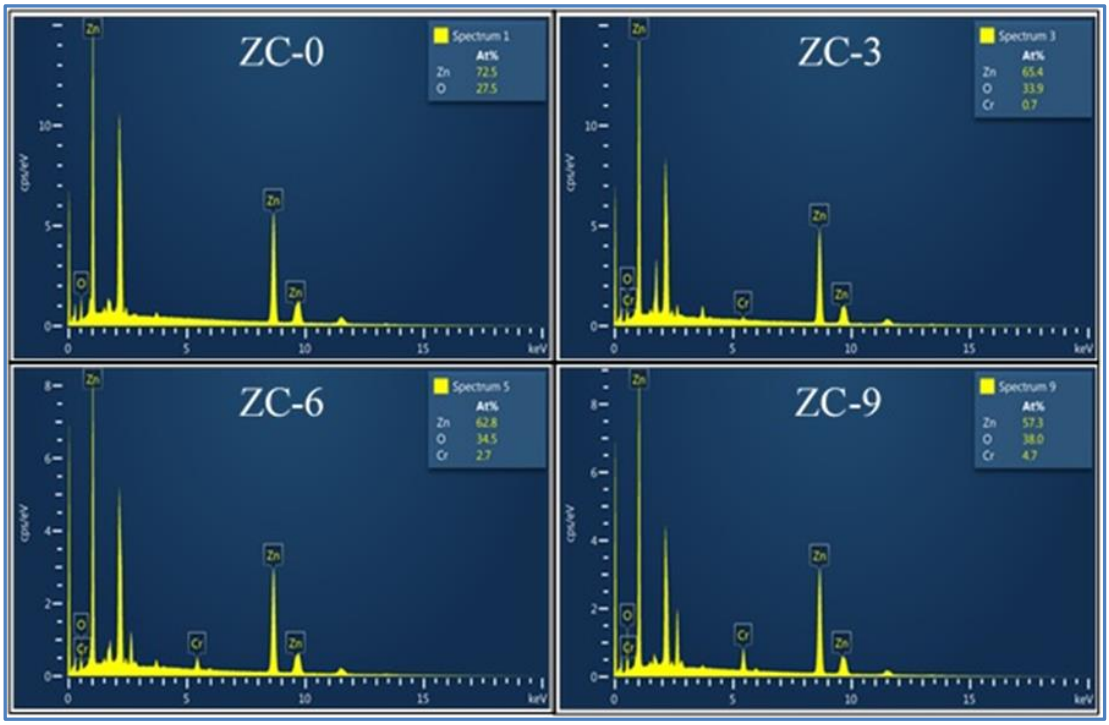

Fig. 4 EDS spectra of ZnO:Cr thin films.

Additionally, with an increasing Cr doping concentration, there is a decrease in the proportion of Zn atoms within the structure.

3.3. Optical Analysis

The optical analyses of undoped and different concentrations of Cr-doped ZnO thin films were conducted by obtaining optical transmittance (*T*), absorbance (*A*), and reflectance (*R*) spectra in the wavelength range of 300 nm to 900 nm (Fig. 5(a-c)). From these spectra, optical band gaps (E_g) and Urbach (E_U) parameters were determined (Fig. 5(d-e)).

The optical transmittance spectra of the thin films are shown in Fig. 5(a). In the visible range (~650 nm), it was determined that the undoped and increasing Cr-doped thin films have transmittance values of approximately 70%, 80%, 80%, and 56%, respectively. This indicates a nearly regular variation in the thin film thicknesses. However, the changes observed in the optical transmittance of the thin films can also be associated with the variation in crystallite sizes, as observed in the structural analyses. The absorbance spectra of the thin films are shown in Fig. 5(b). Upon examining the absorbance spectra of the thin films, it is observed that they exhibit low absorption in the range of 380 nm to 900 nm, with absorbance values ranging from 0.5 to 0.8. There is a sharp increase in absorbance at wavelengths shorter than 380 nm. Accordingly, it is evident that the absorption edge changes in the range of 370 nm to 380 nm. The reflection spectra of the thin films are shown in Fig. 5(c). Upon examining the reflection spectra of the thin films, it was found that they exhibit optical reflection of approximately 9%, 6%, 6%, and 32% in the visible range (~650 nm) for undoped and increasing Cr-doped thin films, respectively. In this regard, it is observed that the surface properties of the thin films significantly influence their reflection values, with smoother surfaces exhibiting higher reflectivity. The optical band gaps of the thin films were determined by plotting $(\alpha h\nu)^2 \sim h\nu$ graphs according to the Tauc's method [22] and are shown in Fig. 5(d).

$$(\alpha h\nu)^2 = A(h\nu - E_g) \quad (5)$$

where E_g is the optical band gap, $h\nu$ is the photon energy, A is a constant, and α is the absorption coefficient. According to this equation, the optical band gaps of the thin films were

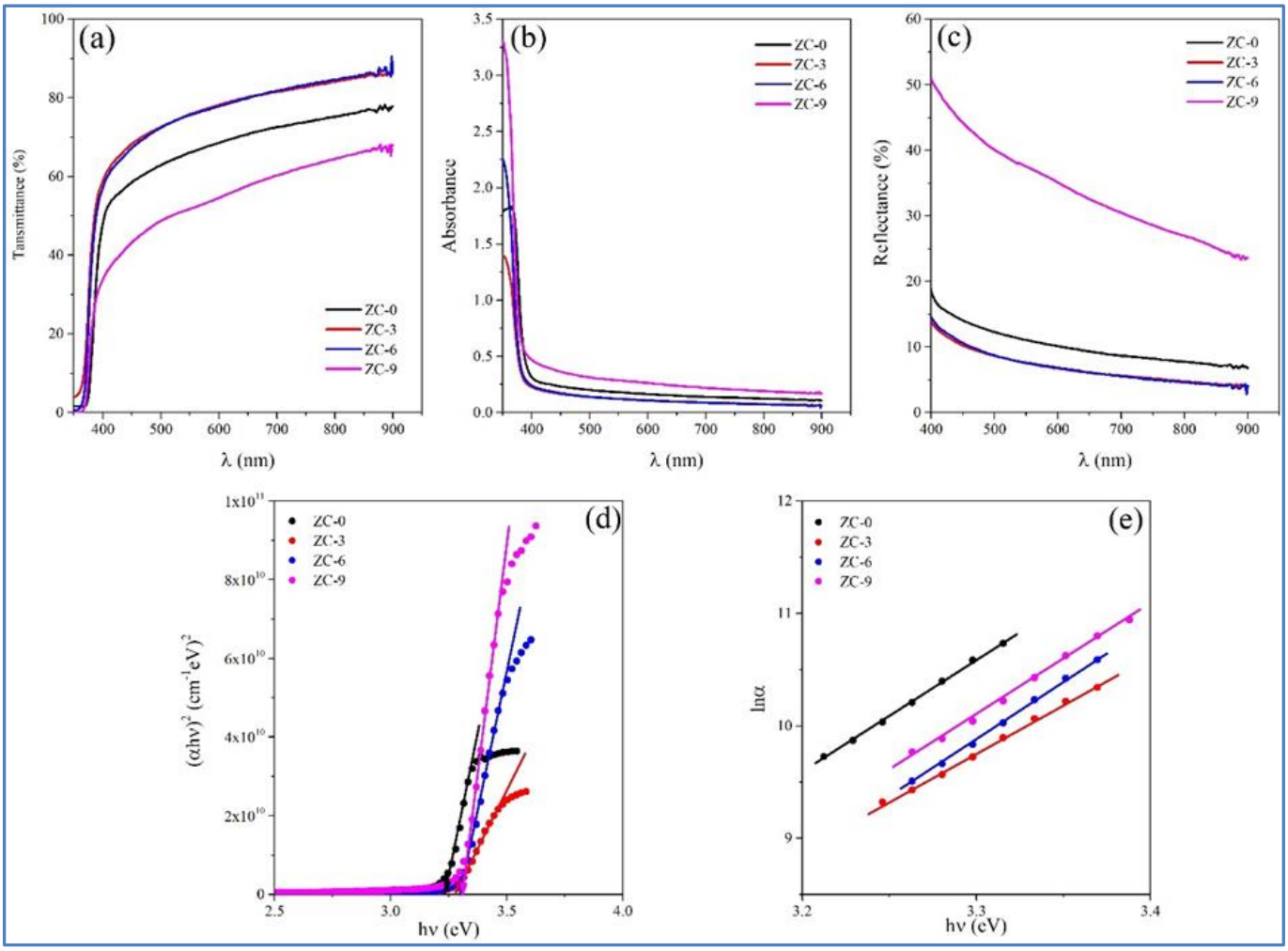

Fig. 5 (a) Transmittance spectra, (b) Absorbance spectra, (c) Reflectance spectra, (d) $(\alpha h\nu)^2 \sim h\nu$ plots, (e) $ln\alpha \sim h\nu$ plots of ZnO:Cr thin films.

determined by using the point where the linear part of the $(\alpha h\nu)^2$ ~ $(h\nu)$ graphs intersects the hν axis. Accordingly, the optical band gaps of the thin films, depending on undoped and increasing Cr doping, were calculated as 3.24 eV, 3.28 eV, 3.30 eV, and 3.31 eV, respectively. It was observed that these values are in good agreement with the data reported in the literature [18,23,24]. In addition, Urbach parameters, which are a measure of band tailing due to localized states within the band gap, were calculated using the slope of ln(α) versus ($h\nu$) graphs in the linear region, as given by the equation [25] below, and presented in Fig. 6(e).

$$\alpha = \alpha_0 exp(h\nu/E_U) \quad (6)$$

where α_0 is a constant, and E_U is the Urbach energy. The Urbach energies of the thin films, depending on undoped and increasing Cr doping, were determined as 99 meV, 113 meV, 96 meV, and 95 meV, respectively. In this regard, it was observed that the Urbach energy shows a relatively higher increase in the ZC-3 thin film due to Cr doping, while there is not a significant change in the other thin films. This increase is believed to be primarily caused by an increase in trap density resulting from the presence of squeezed atoms such as Zn and Cr within the material, as well as an increase in oxygen vacancies within the crystal lattice, accompanying the Cr doping.

3.4. Electrical Analysis

Electrical analysis of the deposited thin films, the type of electrical conductivity was first determined using the hot-probe technique, revealing that all the thin films exhibited n-type electrical conductivity. Subsequently, the electrical resistivity values at room temperature were determined using the four-probe technique (Table 2). Depending on undoped and increasing Cr doping, the electrical resistivity values were found to be $1.38x10^2$ Ωcm, $3.04x10^1$ Ωcm, $2.25x10^5$ Ωcm, and $3.35x10^6$ Ωcm, respectively (Fig. 6). In addition to being in good agreement with the data reported in the literature, it should be noted that some studies have reported even larger values for these parameters [26,27]. Here, it became evident that the electrical resistivity decreased in the ZC-3 thin film, but significantly increased in the ZC-6 and ZC-9 thin films as the doping concentration increased. This phenomenon suggests that the observed changes in the crystal structures of the ZC-6 and ZC-9 thin films, along with a decrease in free carrier density due to the increase in doping ratio, might be the main reasons for this behavior. Moreover, it can be attributed to a relatively smaller crystallite size caused by Cr doping. As a result, the reduction in crystallite size leads to an increase in scattering centers represented by crystallite boundaries, resulting in a decrease in the mobility of free carriers.

4. Conclusion

In this study, the physical properties of Cr-doped ZnO thin films deposited using the low-cost, large-area-coating-capable, and user-friendly ultrasonic spray pyrolysis technique were investigated. Structural analysis revealed that the crystallinity of the thin films changed with the dopant concentration. The intensity of the peak corresponding to the (002) plane initially increased and then decreased, with a subsequent increase, indicating a significant variation in crystallinity at different dopant concentrations. Morphological analysis demonstrated noticeable changes on the film surfaces in conjunction with the dopant. The optical band gaps of the films exhibited a smooth increase from 3.24 eV to 3.31 eV with increasing dopant concentration. The electrical resistivity values of the films varied between $3.04x10^1$ Ωcm and $3.35x10^6$ Ωcm, with a remarkable increase in electrical resistivity observed at high dopant concentrations. These results indicate substantial variations in the physical properties of ZnO thin films with the chromium doping concentration. Further research could address whether these properties can be enhanced for specific applications, posing an important research question. The findings from this study could serve as a valuable reference for various technological applications.

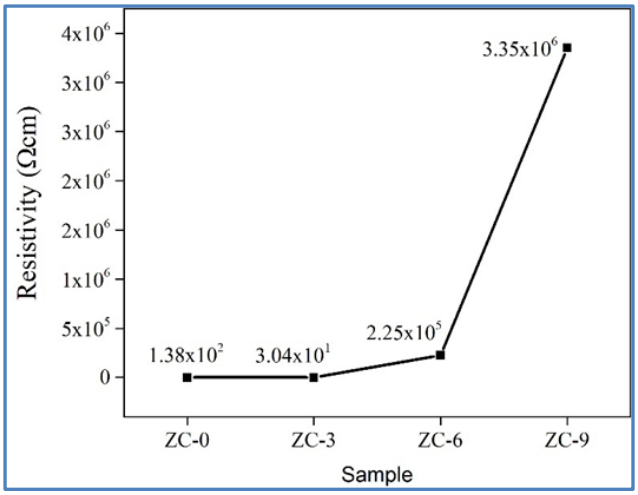

Fig. 6 The variation of resistivity in ZnO:Cr thin films.

Table 2. Optical band gap (E_g), Urbach energy (E_u) and resistivity (ρ) of ZnO:Cr thin films.

Sample	E_g (eV)	E_u (meV)	ρ (Ωcm)
ZC-0	3.24	99	$1.38x10^2$
ZC-3	3.28	113	$3.04x10^1$
ZC-6	3.30	96	$2.25x10^5$
ZC-9	3.31	95	$3.35x10^6$

Declaration

Author Contribution: Conceive- I.G, V.B., E.S.; Design- İ.G., E.S., V.B.; Supervision- V.B., E.S., İ.G.; Experimental Performance, Data Collection and/or Processing- İ.G., E.S.; Analysis and/or Interpretation- İ.G., E.S., V.B.; Literature Review- İ.G., E.S., V.B.; Writer- İ.G., E.S., V.B.; Critical Reviews- İ.G., E.S., V.B.

Acknowledgment: This work was supported by the Canakkale Onsekiz Mart University Scientific Research Projects Committee under the project number FBA-2018-2696.

Conflict of interests: The authors have declared no conflicts of interest.

Orcid-ID

Ibrahim Gunes https://orcid.org/0000-0001-9388-6223
Emrah Sarica https://orcid.org/0000-0002-9339-5114
Vildan Bilgin https://orcid.org/0000-0002-0937-6763

References

[1] A. H. Shah, R. A. Zargar, M. Arora, and P. B. Sundar, "Fabrication of pulsed laser-deposited Cr-doped zinc oxide thin films: structural, morphological, and optical studies," J. Mater. Sci. Mater. Electron., vol. 31, no. 23, pp. 21193–21202, 2020, doi: 10.1007/s10854-020-04632-9.

[2] H. M. Ahmed, Z. M. Abd El-Fattah, N. S. Anad, M. Attallah, and H. H. El-Bahnasawy, "Thermo-mechanical and opto-electrical study of Cr-doped-ZnO-based polyvinyl chloride nanocomposites," J. Mater. Sci. Mater. Electron., vol. 34, no. 2, pp. 1–18, 2023, doi: 10.1007/s10854-022-09412-1.

[3] V. C. Agulto et al., "Low-threshold amplified UV emission of optically pumped ZnO-polymer nanocomposites," J. Cryst. Growth, vol. 573, no. August, p. 126328, 2021, doi: 10.1016/j.jcrysgro.2021.126328.

[4] Ü. Morkoc, H.; Özgür, Wide Bandgap Light Emitting Materials And Devices Liquid Phase Epitaxy of Electronic , Optical and Optoelectronic Materials. 2009.

[5] M. Que, C. Lin, J. Sun, L. Chen, X. Sun, and Y. Sun, "Progress in zno nanosensors," Sensors, vol. 21, no. 16, pp. 1–22, 2021, doi: 10.3390/s21165502.

[6] A. Kolodziejczak-Radzimska and T. Jesionowski, "Zinc oxide-from synthesis to application: A review," Materials (Basel)., vol. 7, no. 4, pp. 2833–2881, 2014, doi: 10.3390/ma7042833.

[7] S. J. Pearton, D. P. Norton, K. Ip, Y. W. Heo, and T. Steiner, "Recent progress in processing and properties of ZnO," Superlattices Microstruct., vol. 34, no. 1–2, pp. 3–32, 2003, doi: 10.1016/S0749-6036(03)00093-4.

[8] M. Benhaliliba, "ZnO a multifunctional material: Physical properties, spectroscopic ellipsometry and surface examination," Optik (Stuttg)., vol. 241, no. May, p. 167197, 2021, doi: 10.1016/j.ijleo.2021.167197.

[9] E. Sarica, I. Gunes, I. Akyuz, V. Bilgin, and K. Erturk, "Sol-gel derived ZnO:Sn thin films and fabrication of n-ZnO:Sn/p-Si heterostructure," Opt. Mater. (Amst)., vol. 118, no. May, p. 111283, 2021, doi: 10.1016/j.optmat.2021.111283.

[10] H. Liu et al., "Single Crystalline Transparent Conducting F, Al, and Ga Co-Doped ZnO Thin Films with High Photoelectrical Performance," ACS Appl. Mater. Interfaces, vol. 15, no. 18, pp. 22195–22203, 2023, doi: 10.1021/acsami.2c22784.

[11] M. Sharma and R. M. Mehra, "Effect of thickness on structural, electrical, optical and magnetic properties of Co and Al doped ZnO films deposited by sol-gel route," Appl. Surf. Sci., vol. 255, no. 5 PART 1, pp. 2527–2532, 2008, doi: 10.1016/j.apsusc.2008.07.153.

[12] Z. Wang, Y. Song, Y. Zhang, and Y. Sui, "Investigation on the comparison of the structural, electrical and optical properties between ZCO:Na and ZCO:(Na, N) films synthesized by RF magnetron sputtering," Ceram. Int., vol. 44, no. 5, pp. 5219–5225, 2018, doi: 10.1016/j.ceramint.2017.12.129.

[13] F. Pan, C. Song, X. J. Liu, Y. C. Yang, and F. Zeng, "Ferromagnetism and possible application in spintronics of transition-metal-doped ZnO films," Mater. Sci. Eng. R Reports, vol. 62, no. 1, pp. 1–35, 2008, doi: 10.1016/j.mser.2008.04.002.

[14] N. S. Anad, Z. M. A. El-Fattah, M. Attallah, H. M. Ahmed, M. M. El-Okr, and H. H. El-Bahnasawy, "Precise determination of optical band gap in Cr-doped semiconductor nanowires," Opt. Quantum Electron., vol. 54, no. 2, pp. 1–14, 2022, doi: 10.1007/s11082-021-03462-1.

[15] M. Laurenti, S. Porro, C. F. Pirri, C. Ricciardi, and A. Chiolerio, "Zinc Oxide Thin Films for Memristive Devices: A Review," Crit. Rev. Solid State Mater. Sci., vol. 42, no. 2, pp. 153–172, 2017, doi: 10.1080/10408436.2016.1192988.

[16] S. Sharma and S. K. Sharma, "Diverse morphology zinc oxide films formulations and characterizations," Nanostructured Zinc Oxide: Synthesis, Properties and Applications. pp. 57–92, 2021, doi: 10.1016/B978-0-12-818900-9.00006-1.

[17] B. D. Cullity, Elements of X-Ray Diffraction. Addison-Wesley Publishing Company, Inc., 1956.

[18] A. Tursucu, S. Aydogan, A. Kocyigit, A. Ozmen, and M. Yilmaz, "Investigation the Performance of Cr-Doped ZnO Nanocrystalline Thin Film in Photodiode Applications," Jom, vol. 74, no. 3, pp. 777–786, 2022, doi: 10.1007/s11837-021-05096-w.

[19] N. H. Al-Hardan, M. J. Abdullah, and A. A. Aziz, "Performance of Cr-doped ZnO for acetone sensing," Appl. Surf. Sci., vol. 270, pp. 480–485, 2013, doi: 10.1016/j.apsusc.2013.01.064.

[20] Z. N. Kayani, M. Siddiq, S. Riaz, and S. Naseem, "Optical, magnetic and structural properties of Cr-doped ZnO thin films by sol-gel dip-coating method," Mater. Res. Express, vol. 4, no. 9, 2017, doi: 10.1088/2053-1591/aa81f1.

[21] A. K. Worku et al., "Structural and thermal properties of pure and chromium doped zinc oxide nanoparticles," SN Appl. Sci., vol. 3, no. 7, 2021, doi: 10.1007/s42452-021-04682-6.

[22] J. Tauc; R. Grigorovici; and A. Vancu, "Optical Properties and Electronic Structure of Ge," phys. stat. sol., vol. 627, pp. 627–637, 1966.

[23] A. Maldonado, S. A. Mallén-Hernández, J. Vega-Pérez, M. De La, L. Olvera, and S. Tirado-Guerra, "Chromium doped Zinc oxide thin films deposited by chemical spray used in photo-catalysis and gas sensing," Rev. Mex. F ´ Isica S, vol. 55, no. 1, pp. 90–94, 2009, [Online]. Available: http://www.redalyc.org/articulo.oa?id=57030347021.

[24] I. Y. Habib, A. A. Tajuddin, H. A. Noor, C. M. Lim, A. H. Mahadi, and N. T. R. N. Kumara, "Enhanced Carbon monoxide-sensing properties of Chromium-doped ZnO nanostructures," Sci. Rep., vol. 9, no. 1, pp. 1–12, 2019, doi: 10.1038/s41598-019-45313-w.

[25] J. I. Pankove, Optical process in semiconductors. New York: Dover Publications, 1975.

[26] R. C. Prajapati, S. Gautam, S. Surve, and V. N. Shukla, “Structural, magnetic, electrical and optical studies of Cr doped nanostructured ZnO thin films for spintronics application,” Mater. Res. Express, vol. 6, no. 10, 2019, doi: 10.1088/2053-1591/ab3879.

[27] G. Mangamma, T. N. Sairam, M. Chitra, and M. Manikandan, “Tailoring the band gap of ZnO nanostructures using chromium,” Phys. B Condens. Matter, vol. 610, no. October 2020, p. 412922, 2021, doi: 10.1016/j.physb.2021.412922.